

## Electronic Supporting Information

### On Structure and Phase Transformation of Uranium Doped $\text{La}_2\text{Hf}_2\text{O}_7$ Nanoparticles as an Efficient Nuclear Waste Host

Maya Abdou<sup>1</sup>, Santosh K. Gupta<sup>1,2</sup>, Jose P. Zuniga<sup>1</sup>, and Yuanbing Mao<sup>1,3\*</sup>

<sup>1</sup>Department of Chemistry, University of Texas Rio Grande Valley, 1201 West University Drive, Edinburg, Texas 78539, USA

<sup>2</sup>Radiochemistry Division, Bhabha Atomic Research Centre, Trombay, Mumbai, 400085, India

<sup>3</sup>School of Earth, Environmental, and Marine Sciences, University of Texas Rio Grande Valley, 1201 West University Drive, Edinburg, Texas 78539, USA

\*To whom correspondence should be addressed. E-mail: yuanbing.mao@utrgv.edu, Tel.: +1-956-665-2986.

#### S.1 Synthesis

More specifically, lanthanum nitrate hexahydrate ( $\text{La}(\text{NO}_3)_3 \cdot 6\text{H}_2\text{O}$ , 99.0%), hafnium dichloride oxide octahydrate ( $\text{HfOCl}_2 \cdot 8\text{H}_2\text{O}$ , 98%), and uranyl nitrate hexahydrate ( $\text{UO}_2(\text{NO}_3)_2 \cdot 6\text{H}_2\text{O}$ , 98-102%) were purchased and used as reactants with no further purifications. The reactants were measured stoichiometrically as  $(5-x)$  mmol of  $\text{La}(\text{NO}_3)_3 \cdot 6\text{H}_2\text{O}$ ,  $x$  mmol of  $\text{UO}_2(\text{NO}_3)_2 \cdot 6\text{H}_2\text{O}$ , and 5 mmol of  $\text{HfOCl}_2 \cdot 8\text{H}_2\text{O}$ , and dissolved in 200 ml of water (Millipore, 18.2 M $\Omega$  at 25°C) with continues stirring. The obtained solution was then titrated with 200 ml of 10% ammonia solution ( $\text{NH}_4\text{OH}$ , 28-30%) for 2h. The resulting precursors were then washed, vacuum filtrated, and dried at 90°C overnight. Sodium nitrate ( $\text{NaNO}_3$ , 98%), potassium nitrate ( $\text{KNO}_3$ , 99%), and the co-precipitated single-source precursor were measured in a ratio of 30:30:1, and ground together using mortal and pestle into fine powder. The resulting powder was annealed in a furnace at 650°C for 6h. The final product was then washed with DI water several times and dried. Finally, fine white to yellow (with increasing uranium content) powders of the  $\text{La}_2\text{Hf}_2\text{O}_7$ : $x\text{mol}\%$ U NPs ( $x = 0.5 - 10.0$ ) were obtained.

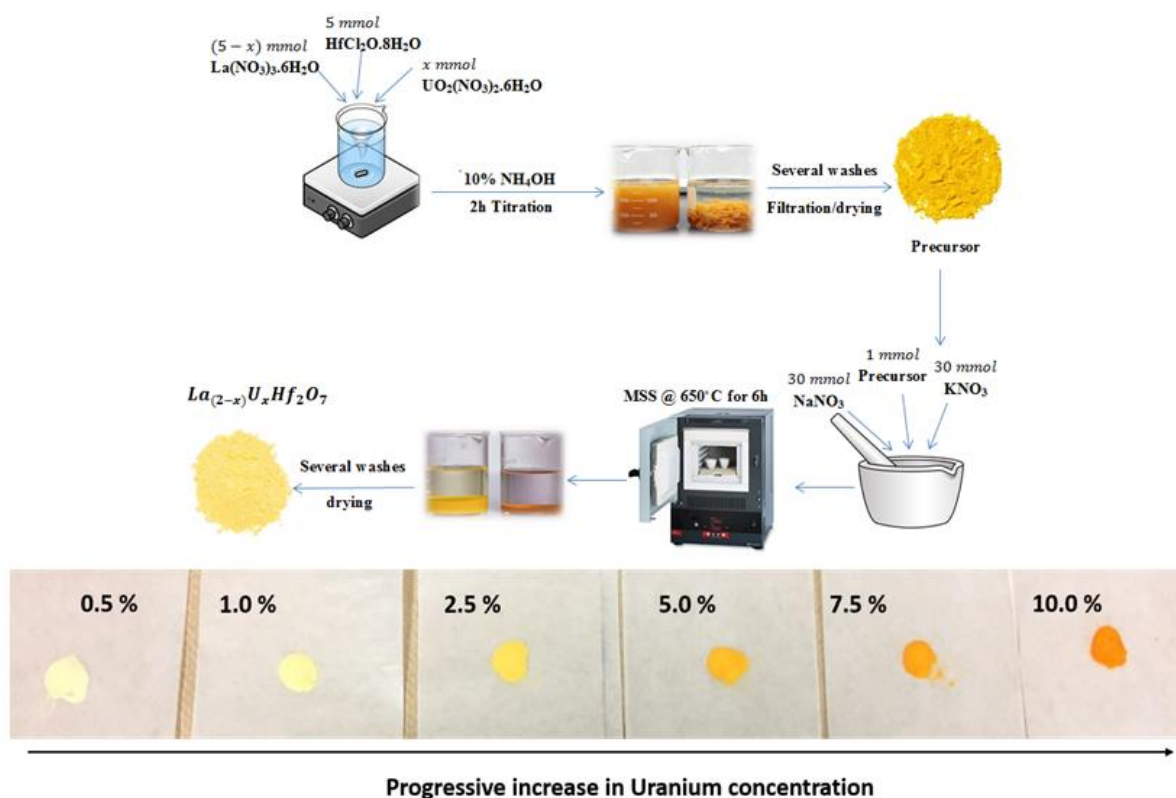


**Figure S1.** Schematic of the combined co-precipitation and MSS procedure for the  $\text{La}_2\text{Hf}_2\text{O}_7\text{:}x\text{mol}\%\text{U}$  ( $x = 0.5 - 10.0$ ) NPs. The lower part of the figure shows the color variation of the as-prepared  $\text{La}_2\text{Hf}_2\text{O}_7\text{:}x\text{mol}\%\text{U}$  NPs as the uranium concentration was varied between 0.5% to 10.0%.

## S.2 Characterization

To ensure their purity and confirm the crystallographic structure of the obtained  $\text{La}_2\text{Hf}_2\text{O}_7\text{:}x\%\text{U}$  ( $x = 0, 0.5, 1, 2.5, 5, 7.5$ , and  $10$ ) NPs, various characterizations were performed. X-ray diffraction (XRD) studies were carried out with BRUKER<sup>TM</sup> D8 X-ray Diffractometer with a  $\text{Cu } K_{\alpha 1}$  radiation ( $\lambda = 0.15406 \text{ nm}$ ,  $40 \text{ kV}$ ,  $40 \text{ mA}$ ) by a  $2\theta$  scanning mode ranging from  $10^\circ$  to  $90^\circ$  and a scanning step size of  $0.04^\circ$  at a scanning rate of  $2.0^\circ \text{ min}^{-1}$ . The structural characteristics of the  $\text{La}_2\text{Hf}_2\text{O}_7\text{:}x\%\text{U}$  NPs were further investigated using a Renishaw 2000 Micro-Raman spectroscopy equipped with an argon laser ( $514.5 \text{ nm}$ ) in the range of  $200\text{--}1000 \text{ cm}^{-1}$ . FTIR spectra were obtained through a Thermo Nicolet Nexus<sup>TM</sup> 470 FTIR system. The microstructure and morphology of the NPs were studied using a Carl Zeiss sigma VP scanning electron microscopy (SEM) equipped with a field emission gun operated at  $5 \text{ kV}$ . Photoluminescence (PL), emission, excitation and time resolved emission spectroscopy (TRES) were measured using an Edinburgh Instruments FLS980 fluorometer system equipped with a steady state xenon source and a pulse xenon source (with a

frequency range of 1-100 Hz). HRTEM was recorded using Hitachi HF 3300 TEM/STEM. XPS measurement was carried out on Scienta Omicron ESCA 2SR.

### S.3 XRD

The XRD patterns of the synthesized  $\text{La}_2\text{Hf}_2\text{O}_7:x\%\text{U}$  ( $x = 0, 0.5, 1, 2.5, 5, 7.5$ , and  $10$ ) NPs (**Figure S2a**) show nine major identifiable diffraction peaks with (hkl) values of (222), (400), (440), (622), (444), (800), (662), (840), and (844). They are well in agreement with the reflections of defect fluorite structure (space group =  $Fm\bar{3}m$ , JCPDS No. 78-1292). Observations were notice that the incorporation of uranium into the  $\text{La}_2\text{Hf}_2\text{O}_7$  host did not distorted the basic host structure. However, it should be noted that XRD sometimes fail to sense the presence of weak pyrochlore reflections, which should be confirmed with further structural analysis by other techniques including FTIR and Raman spectroscopy.

There is a progressive decrease of the lattice parameter as a function of uranium doping concentration of the synthesized  $\text{La}_2\text{Hf}_2\text{O}_7:x\%\text{U}$  NPs (**Figure S2b**). This is because the ionic radius of 8-coordinated uranium ion (86 pm) is smaller than that of 8-coordinated  $\text{La}^{3+}$  ion (116 pm). There is a reduction of the crystallite size, calculated using Debye-Scherrer formula, as a function of uranium doping concentration of the synthesized  $\text{La}_2\text{Hf}_2\text{O}_7:x\%\text{U}$  NPs (**Table S1**). This can be attributed to the difference of the ionic radii between  $\text{La}^{3+}$  and U ions and the size mismatch between lattice La/Hf sites and uranium ion. Crystallite size diminished because of the lattice distortion caused by radius difference between the uranium ion and the replaced La/Hf ion. The calculated crystallite sizes are between 16-25 nm indicating the formation of  $\text{La}_2\text{Hf}_2\text{O}_7:x\%\text{U}$  NPs by our synthesis procedure.

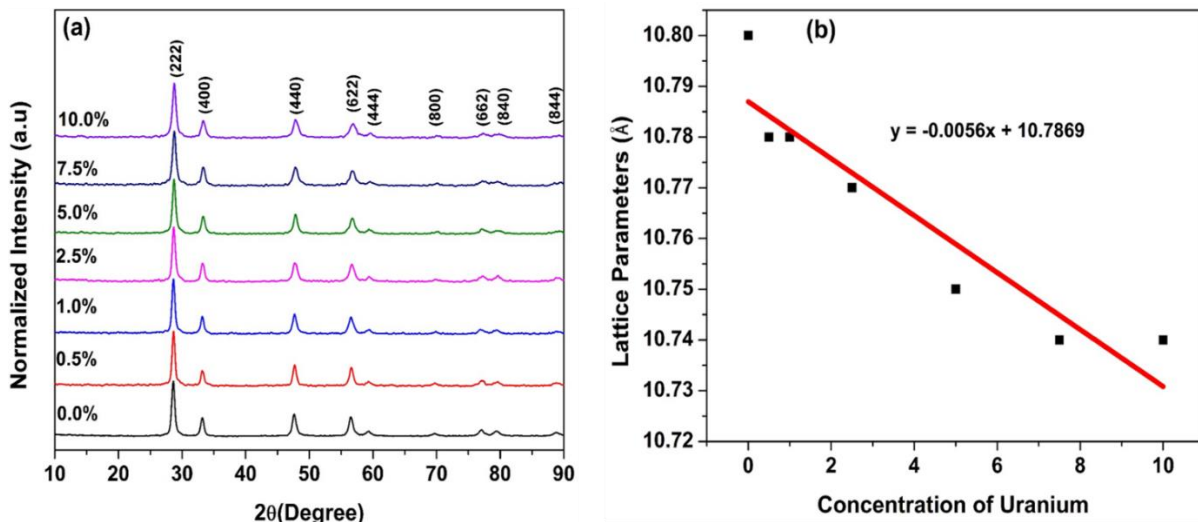


**Figure S2.** (a) XRD patterns and (b) variation of lattice parameter as a function of the uranium doping concentration of the La<sub>2</sub>Hf<sub>2</sub>O<sub>7</sub>:x%U (x = 0, 0.5, 1, 2.5, 5, 7.5, and 10) NPs.

**Table S1.** Variation in lattice parameter and crystallite size of the La<sub>2</sub>Hf<sub>2</sub>O<sub>7</sub>:x%U NPs as a function of uranium doping concentration

La <sub>2</sub> Hf <sub>2</sub> O <sub>7</sub> :x%U	2θ (°)	FWHM (β)	Lattice parameters (Å)	Particle size (nm)
0.0	28.62	0.35	10.80	22.70
0.5	28.66	0.32	10.78	24.83
1.0	28.65	0.33	10.78	24.07
2.5	28.70	0.37	10.77	21.47
5.0	28.74	0.40	10.75	19.86
7.5	28.78	0.47	10.74	16.90
10.0	28.77	0.49	10.74	16.21

#### S.4 FTIR

Since the bending and stretching vibrations of the metal–oxygen bonds induce infrared active optic modes, FTIR spectroscopy has been used to study the nature of the M-O bonds in the A<sub>2</sub>B<sub>2</sub>O<sub>7</sub> compounds. Subramanian and the group reported that the infrared spectra of A<sub>2</sub>B<sub>2</sub>O<sub>7</sub> type oxides consist of seven infrared modes in the range of 750–50 cm<sup>-1</sup> originating from bending and vibration of the M-O bonds.<sup>1</sup> As shown in the FTIR spectra of the La<sub>2</sub>Hf<sub>2</sub>O<sub>7</sub>:x%U (x = 0, 0.5, 1, 2.5, 5, 7.5, and 10) NPs (**Figure S3**), the infrared band around 610 cm<sup>-1</sup> (ν<sub>3</sub>) is attributed to the Hf-O stretching in the HfO<sub>6</sub> octahedra and the one at ~426 cm<sup>-1</sup> (ν<sub>1</sub>) to the La-O stretching in the LaO<sub>8</sub>

scalenohedra.<sup>2</sup> The peak at 521  $\text{cm}^{-1}$  ( $\nu_2$ ) corresponds to Hf-O' bond. Thus FTIR spectra further confirmed the presence of  $\text{LaO}_8$  and  $\text{HfO}_6$  moieties, and these vibrations confirmed the formation of  $\text{La}_2\text{Hf}_2\text{O}_7$  structure. On uranium doping, the  $\nu_2$  and  $\nu_3$  IR bands merged with the creation of a single broadband at 500  $\text{cm}^{-1}$ , which underwent blue shift at higher doping concentrations. The  $\nu(\text{Hf-O})$  shifted to low frequency with increasing uranium doping concentration, indicating the Hf-O bond strength weakened. This is attributed to decreasing Hf-O distance as uranium doping concentration increases. This effect is even more pronounced at higher uranium doping concentration. It can be attributed to identity change of uranium ion from  $\text{U}^{4+}$  to  $\text{UO}_6^{6-}$ . Indeed, this is related to the pyrochlore to cotunnite structural transformation, which was further confirmed using Raman spectroscopy as discussed below.

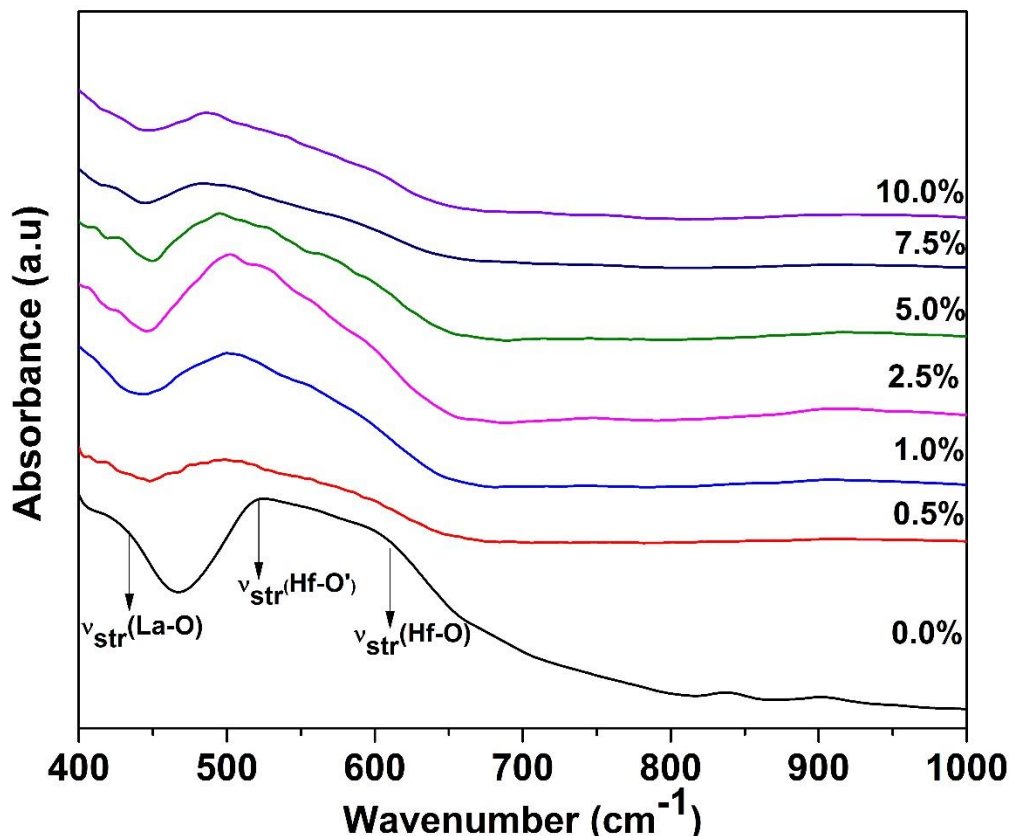


**Figure S3.** FTIR spectra of the  $\text{La}_2\text{Hf}_2\text{O}_7\text{:x}\%\text{U}$  ( $x = 0, 0.5, 1, 2.5, 5, 7.5$ , and  $10$ ) NPs.

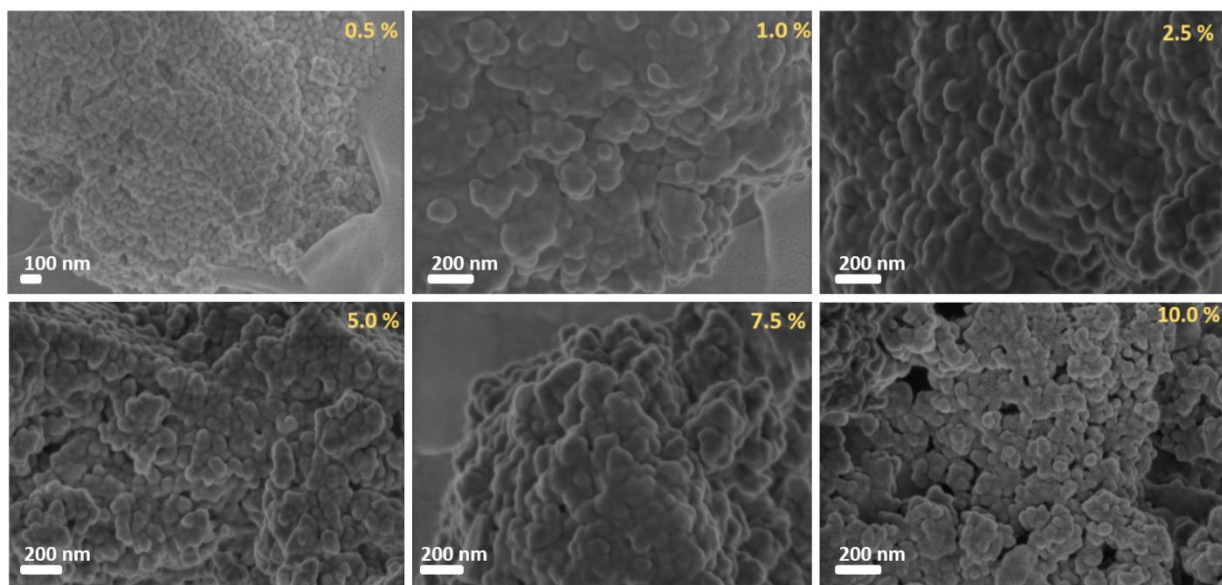
## S.5 SEM

**Figure S4** shows the SEM images of the  $\text{La}_2\text{Hf}_2\text{O}_7\text{:x}\%\text{U}$  ( $x = 0.5, 1, 2.5, 5, 7.5$ , and  $10$ ) NPs. The SEM micrographs show the formation of nanospheres with an average diameter of  $\sim 30$  nm, which is in close agreement with the calculated crystallite size using the Debye-Scherrer equation from the XRD

data (Figure 2a). All SEM images clearly showed that the as-synthesized particles are in nanodomain and spherical in shape. However, there is certain degree of agglomeration in all of these samples. High surface area to volume ratio of nanoparticles provides a very high surface energy. To minimize its surface energy the nanoparticles tends to agglomerate. Uncontrolled agglomeration of nanoparticles may occur due to attractive van der Waals forces between particles. The morphology of these NPs remain the same well-defined grain boundaries even at 10.0% uranium doping level showing the capability of our synthesis procedure.

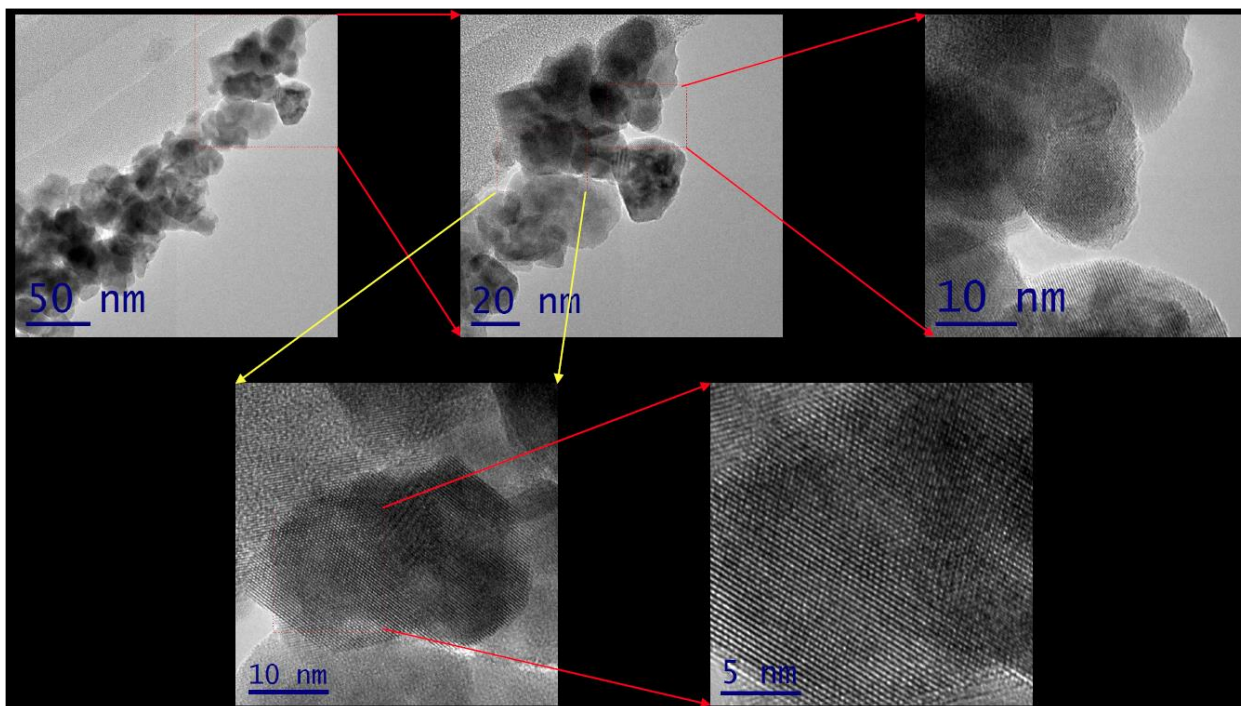
Furthermore, the nano-sized NPs and their actual morphology are also confirmed using high-resolution transmission electron microscopy (HRTEM). As a representative  $\text{La}_2\text{Hf}_2\text{O}_7:10\%\text{U}$  NPs is shown in **Figure S5**. The particles are slightly aggregated, with while individual particles are in nano-domain and are concordant with SEM results showing most of the particles as spheres.

EDS analysis shown in **Figure S6** clearly confirms the presence of La, Hf, O and U in  $\text{La}_2\text{Hf}_2\text{O}_7:10\%\text{U}$  NPs and no traces of any other impurity could be seen in the synthesized NPs indicating their high purity. The energy dispersive spectroscopy (EDS) method is used to evaluate the composition uniformity of uranium ion in doped  $\text{La}_2\text{Hf}_2\text{O}_7:10\%\text{U}$  NPs. **Figure S7a** and **b** show the EDS combined as well as individual elemental mapping image of  $\text{La}_2\text{Hf}_2\text{O}_7:10\%\text{U}$  NPs respectively. From this figure it is clearly seen that all elements are very homogeneously distributed within the lanthanum hafnate nano particles, and there is no signature of any impurity, which further proves that uranium ion has been successfully incorporated into lanthanum hafnate nano particles to form the isostructural solid solutions.

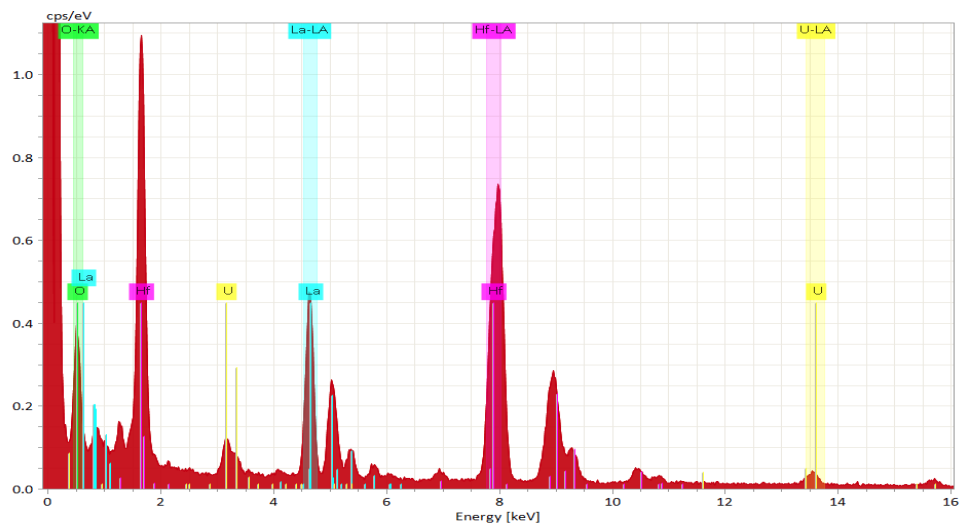




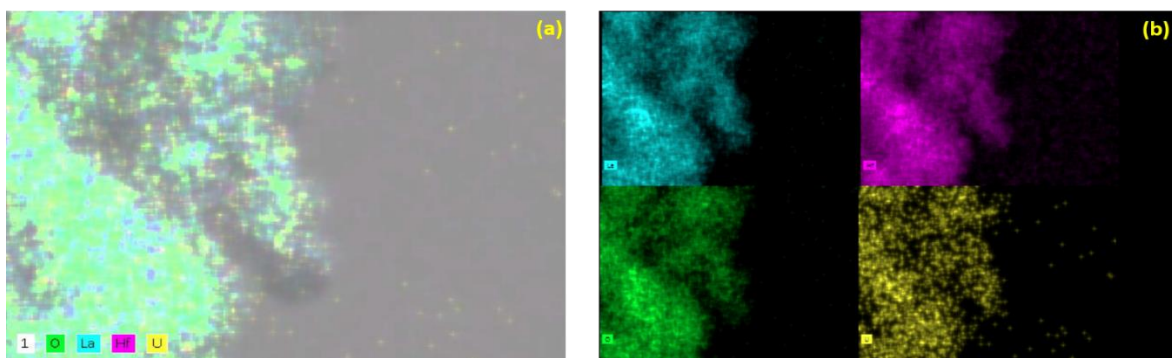
**Figure S4.** SEM images of  $\text{La}_2\text{Hf}_2\text{O}_7:10\%\text{U}$  NPs with different uranium doping concentrations of  $x = 0, 0.5, 1, 2.5, 5, 7.5$ , and 10. Number with percentage in the SEM graphs indicate the uranium doping levels.



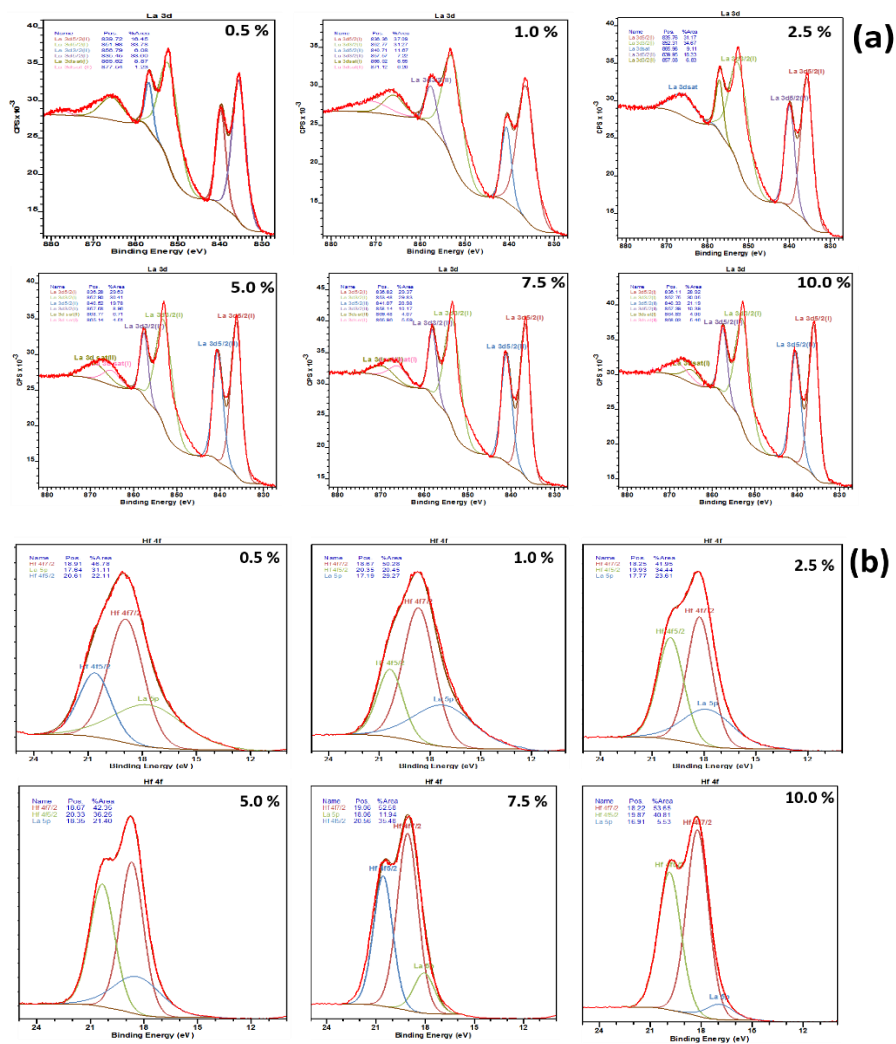
**Figure S5.** HRTEM images of  $\text{La}_2\text{Hf}_2\text{O}_7:10\%\text{U}$  NPs under different magnification.



**Figure S6.** EDS spectrum of  $\text{La}_2\text{Hf}_2\text{O}_7:10\%\text{U}$  NPs.



**Figure S7.** (a) EDS elemental combined and (b) Individual elemental mapping of the  $\text{La}_2\text{Hf}_2\text{O}_7:10\%\text{U}$  NPs.





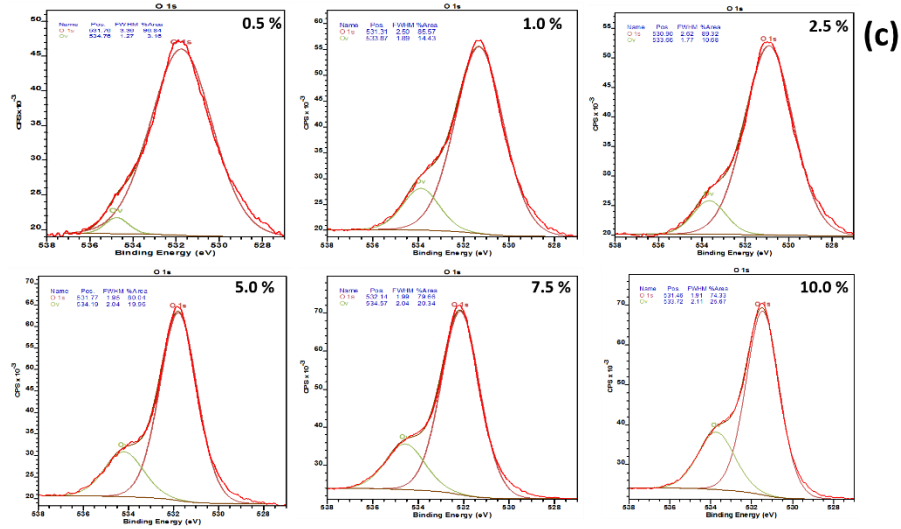


**Figure S8.** (a) XPS spectra for core electrons of (a) La 3d, (b) Hf 4f, and (d) O 1s of the  $\text{La}_2\text{Hf}_2\text{O}_7:x\%\text{U}$  ( $x = 0.5, 1.0, 2.5, 5.0, 7.5$ , and  $10.0$ ) NPs.

**Table S2.** Various XPS parameter of uranium ion in  $\text{La}_2\text{Hf}_2\text{O}_7:\text{U}$

Uranium doping level (mol %)	Binding energy $\text{U}^{4+}$ (eV)	Binding energy $\text{U}^{6+}$ (eV)	Integrated area of $7f_{5/2} \text{U}^{4+}$	Integrated area of $7f_{5/2} \text{U}^{6+}$	$\text{U}^{4+}/\text{U}^{6+}$ ratio
2.5	392.31	3.93.16	656.19	606.11	1.08
5.0	393.00	393.83	1653.71	3484.60	0.47
7.5	393.52	394.40	1942.46	6278.58	0.31
10.0	392.89	393.76	3003.04	10111.93	0.29

### Information I1:

Therefore, we applied biexponential fitting equation to fit the profile:

$$I(t) = B_1 \exp\left(-\frac{t}{\tau_1}\right) + B_2 \exp\left(-\frac{t}{\tau_2}\right)$$

where  $I(t)$  is the emission intensity,  $\tau_1$  and  $\tau_2$  are luminescence decay times, and  $B_1$  and  $B_2$  are their relative magnitude.

The percentage of individual lifetime is calculated using following equation:

$$\% \tau_1 = \frac{B_1 \tau_1}{B_1 \tau_1 + B_2 \tau_2} \times 100$$

$$\% \tau_2 = \frac{B_2 \tau_2}{B_1 \tau_1 + B_2 \tau_2} \times 100$$

## References:

1. Subramanian, M.; Aravamudan, G.; Rao, G. S., Oxide pyrochlores—a review. *Progress in Solid State Chemistry* **1983**, *15*, 55-143.
2. Wang, Z.; Zhu, H.; Ai, L.; Liu, X.; Lv, M.; Wang, L.; Ma, Z.; Zhang, Z., Catalytic combustion of soot particulates over rare-earth substituted  $\text{Ln}_2\text{Sn}_2\text{O}_7$  pyrochlores (Ln= La, Nd and Sm). *Journal of colloid and interface science* **2016**, *478*, 209-216.